Nano Research 2016, 9(11): 3355–3363
DOI 10.1007/s12274-016-1213-8
Research Article
ISSN 1998-0124
CN 11-5974/O4

Double-induced-mode integrated triboelectric nanogenerator based on spring steel to maximize space utilization

Guanlin Liu[1], Hengyu Guo[1], Lin Chen[1], Xue Wang[1], Dapeng Wei[2], and Chenguo Hu[1] (✉)

[1] *Department of Applied Physics, Chongqing University, Chongqing 400044, China*
[2] *Chongqing Engineering Research Center of Graphene Film Manufacturing, Chongqing 401329, China*

Received: 13 June 2016
Revised: 10 July 2016
Accepted: 13 July 2016

KEYWORDS
triboelectric nanogenerator,
double-induced-mode,
spring steel,
stackable rhombus structure

ABSTRACT

Integrated multilayered triboelectric nanogenerators (TENGs) are an efficient approach to solve the insufficient energy problem caused by a single-layered TENG for achieving high output power density. However, most integrated multilayered TENGs have a relatively large volume. Here, a double-induced-mode integrated triboelectric nanogenerator (DI-TENG) based on spring steel plates is presented as a cost-effective, simple, and high-performance device for ambient vibration energy harvesting. The unique stackable rhombus structure, in which spring steel plates act both as skeletons and as electrodes, can enhance the output performance and maximize space utilization. The DI-TENG with five repeated units in a volume of 12 cm × 5 cm × 0.4 cm can generate a short-circuit current of 51 μA and can transfer charges of 1.25 μC in a half period. The contrast experiment is conducted systematically and the results have proved that the DI-TENG has a great advantage over the single-induced-mode TENG (SI-TENG) with only one side of a friction layer on its electrode. Besides, the DI-TENG can easily power a commercial calculator and can be used as a door switch sensor.

1 Introduction

Along with the rapid increase in electronic devices and systems, there will be a huge demand for supplying power for them; since there will be trillions of sensor units distributed on the Earth by 2020 [1]. The idea of harvesting vibration energy from the ambient environment is a brilliant solution to the problem, not only providing sustainable maintenance-free power sources but also reducing environmental pressure from batteries. Among a number of technologies that can convert mechanical energy to electricity [2–8], triboelectric nanogenerators (TENGs) have been developed aiming at building up self-powered systems to drive small electronic devices [9–13]. With TENG, an outstanding total energy conversion efficiency up to 85%, an instantaneous conversion efficiency of 70% and an output area power density up to 500 $W \cdot m^{-2}$

Address correspondence to hucg@cqu.edu.cn

have been achieved [14–16].

Based on the coupling of contact electrification effect and electrostatic induction, TENG has experienced a rapid development by the efforts of over 40 groups around the world [10, 17]. There are mainly four working modes of TENGs, including the vertical contact-separation mode [18–23], the lateral sliding mode [24–26], the single-electrode mode [27–29], and the free-standing mode [30–32]. These reveal a great potential in energy harvesting applications for almost any kind of mechanical motion, such as walking [33–35], breathing [36], wheel spinning [37–39], and ocean energy [40, 41]. However, achieving a higher output through an innovative structure design is still a challenging task, while the integration of individual TENGs is expected to have an efficient and feasible approach. Unfortunately, most previous integrated TENGs have relatively large volume due to the requirement of a support material, which hinders the application of TENGs [29, 42–48].

Herein, we design a novel double-induced-mode integrated triboelectric nanogenerator (DI-TENG) that uses spring steel plates. The spring steel plate works as both the skeleton and the electrode in DI-TENG and saves a lot of space and material to maximize space utilization. The DI-TENG only gets an additional thickness of 4 mm when five units are integrated. More importantly, two tribo-layers can stick to a spring steel plate on both sides in the integrated TENG, which greatly improves the output performance and completely distinguishes itself from most previous TENGs. Such a unique double-induced-mode integrated structure working in the contact-separation mode can provide higher energy conversion efficiency than that of single-induced-mode integrated triboelectric nanogenerator (SI-TENG). The output current of DI-TENG is 199% and the transferred electric charge is 68% higher than that of SI-TENG. The maximum short-circuit current, open-circuit voltage, and output power are 51 μA, 418 V, and 2.16 mW, respectively, which is strong enough to light tens of commercial LED lights and to power a commercial calculator. In addition, the DI-TENG is successfully applied to a door switch sensor that can turn the mechanical switch signal into electric signal without additional power supply. The electricity generation mechanism of the double-induced mode and some of the factors that influence the output of TENG are discussed in detail. The creative idea of using spring steel plates in the integration of TENG units would lead to a new structure/material design for TENGs.

2 Experimental

2.1 Fabrication of DI-TENG

The device structure of the DI-TENG is schematically illustrated in Fig. 1. The DI-TENG is made up of bare spring steel plates and the spring steel plates are covered with polytetrafluoroethylene (PTFE) on their surfaces. Spring steel plates have favorable features like suitable flatness, good elasticity, a well-polished surface, and fatigue-resistance. The two kinds of plates (the bare plate and the sandwiched plate) were alternately stacked together. All the bare spring steel plates were connected together by copper wires to form a M electrode. The sandwiched spring steel plates covered with PTFE were connected to form a P electrode. In order to protect the device and operate it easily, we added acrylic plates on the top and bottom of the DI-TENG.

M electrode: We cut the commercial spring steel plate (Kobetool, Germany, width 25 mm, length 5,000 mm, and thickness 0.15 mm) into slices of lengths (120 mm). Ethanol spray treatment was then performed to remove any oil, after which they were dried at 40 ℃. These slices were connected together with copper wires, of which each works as an electrode.

P electrode: A commercial spring steel plate with a thickness of 0.10 mm was cut into slices of 120-mm length, and after ethanol spray treatment and drying, each slice was covered on both sides with commercial PTFE film (thickness 0.1 mm) as tribo-layers using double-sided adhesive (thickness 0.104 mm). Figure 1(b) shows a schematic diagram of a unit in DI-TENG, and Fig. 1(c) shows a scanning electron microscopy (SEM) image of the PTFE thin-film surface. Similarly, these spring steel plates were connected with copper wires on one end. Each spring steel plate works as another electrode.

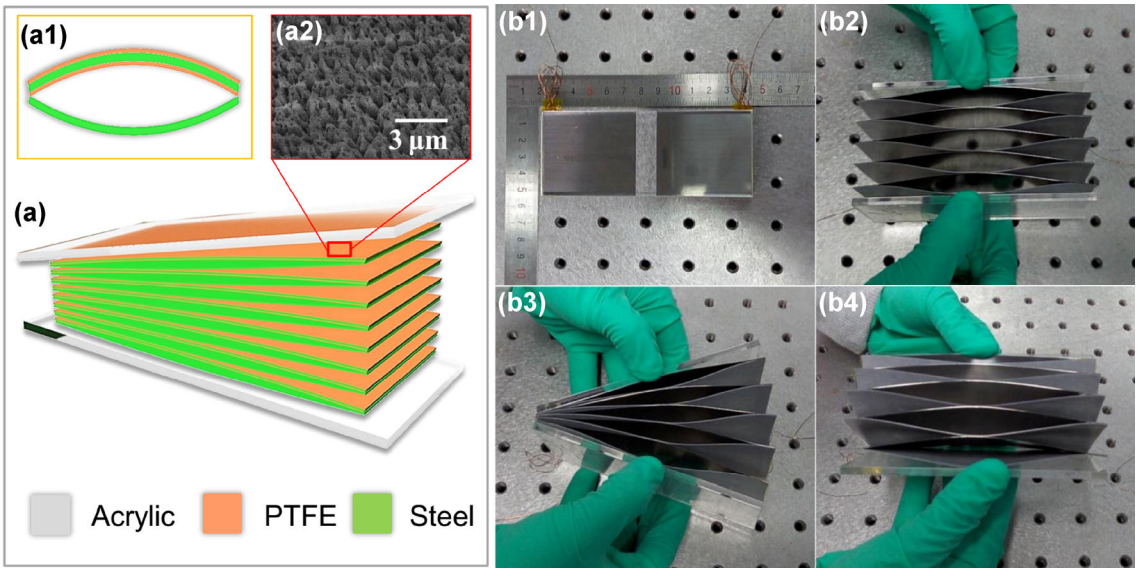

Figure 1 Double-induced-mode integrated triboelectric nanogenerator. (a) Schematic diagram of a DI-TENG. (a1) Schematic diagram of the unit cell in DI-TENG; (a2) SEM image of the etched PTFE surface with nanowire-like structure. (b) Photograph of DI-TENG with five units under different conditions: (b1) free initial state; (b2) stretch; (b3) bend; (b4) bend in another direction.

2.2 Characterization of DI-TENG

The output performance of the DI-TENG was measured using a preamplifier (Keithley 6514 System Electrometer) and a Data Acquisition Card (NI PCI-6259). In the experiment, we fix the acryl boards of DI-TENG respectively onto the motion module and stator of the linear motor (WMU1536075-090-D).

3 Results and discussion

It has been a great dream of researchers to invent a nanogenerator that produces high output with a small volume. Based on specific elasticity and conductivity of the spring steel, which can be used both as an electrode and as a skeleton to support tribo-layers on both sides, an integrated TENG with a relatively small volume can be achieved by assembling such spring steel units. The spring steel plate covered by PTFE films on both sides can work on a double-induced-mode, where the electron transfer on electrodes can be induced by the bound charges on two PTFE tribo-layers. With the unique stacked layer structure, the DI-TENG can be stretched to a series rhombus from side view in any direction, as shown in Fig. 1. The degree of the stretch and the bend angle can be further improved with more units (Fig. S1 in the Electronic Supplementary Material (ESM)). Besides, the thickness of DI-TENG is specifically small, 0.4 cm with 5 units and 1.2 cm with 15 units, as exhibited in Fig. S2 (in the ESM). To better understand the importance of P electrode with two-side friction layers, we have fabricated a SI-TENG for comparison, that is, a polyethylene glycol terephthalate (PET) film is used to replace the PTFE film on one side of the P electrode. Since the structure of the DI-TENG and the SI-TENG is similar, we draw two semi-graphs (left and right) for them in one schematic diagram to illustrate the difference of the charge distribution and current flowing during the working process (Fig. 2(a)). A detailed illustration of charge distribution for these two TENGs is separately shown in Fig. S3 (in the ESM). The stable charge distribution and current generating procedure are shown in Fig. S4 (in the ESM) after the two TENGs have been working for several cycles, where an equal amount of positive and negative charges is generated on the PTFE film and spring steel plates, respectively. When we pull the acrylic plates to separate M and P electrodes, the negative charges on the PTFE films induce an amount of positive charge in the spring steel plate of the P electrode, which produces a current flowing from M electrode to P electrode (Fig. 2(a), top). Subsequently, after

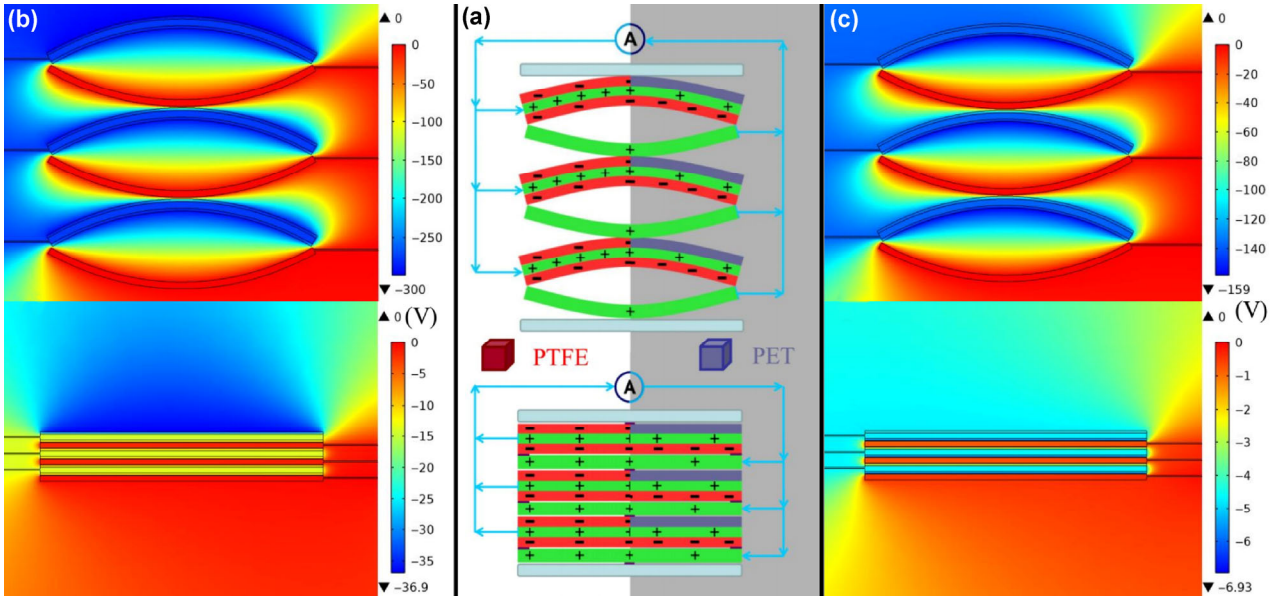

Figure 2 Schematics of the operating principle of TENG in separation state (top) and contact state (bottom). (a) Two schematic illustrations of the charge distribution that have been scheduled in one picture, the bright side (left) is for DI-TENG and the shaded side (right) is for SI-TENG. Potential distribution by COMSOL is employed to elucidate the working principle of (b) the DI-TENG in a period and (c) the SI-TENG in a period.

reaching the maximum displacement position, we release the acrylic plates to let the M and P electrodes contact, and thus the negative charges on the PTFE films induce the positive charges in the M electrode. This results in a current from P electrode to M electrode (Fig. 2(a), bottom). The TENG working in continuous cycles generates an alternating current in the external circuit. From Fig. 2(a), we can intuitively see that the amount of charge transferred from DI-TENG is larger than that from SI-TENG due to the double-induced-mode. It is important that every unit contacts each other synchronously but separates in different steps, which can be inferred from the current-time waveform (Fig. S5(a) in the ESM). Moreover, Comsol multiphysics software based on finite-element simulation is employed to calculate the potential distribution in the two TENGs under open-circuit conditions, as shown in Fig. 2(b) (DI-TENG) and Fig. 2(c) (SI-TENG), in which all the spring steel plates with PTFE film are connected together to work as an electrode and all the bare spring steel plates are connected together to serve as another electrode. In brief, the electric potential difference of the two electrodes in DI-TENG is theoretically much higher than that of the ones in SI-TENG.

To evaluate the two TENGs' performance for harvesting vibration energy experimentally, a linear motor that provides a sinusoidal wave is employed as an external vibration source with tunable period (T) and amplitude (A), which are both key factors to output performance. The experimental measurement results are shown in Fig. 3, where the color contour graphs are all smoothened by bilinear interpolation algorithm, revealing the output current ((a) and (b)) and the quantity of transferred charges in a half period ((c) and (d)) for the DI-TENG ((a) and (c)) and SI-TENG ((b) and (d)), under different motion periods and amplitudes. There are 3D color graphs, and 2D graphs derived from corresponding 3D graphs as depicted in Figs. S6 and S7 (in the ESM), which demonstrate the same result in detail as Fig. 3. It should be noted that Figs. 3(a) and 3(b) share the same color scale, while Figs. 3(c) and 3(d) share another color scale. In Figs. 3(a) and 3(b) we can intuitively see that the output current increases with a decrease in period or an increase in amplitude, and the output current of DI-TENG is 2.99 times as much as that of SI-TENG. Due to the integrated multilayer structure, the motion velocity of acrylic plate is divided to a smaller velocity on each electrode. In other words, each electrode has

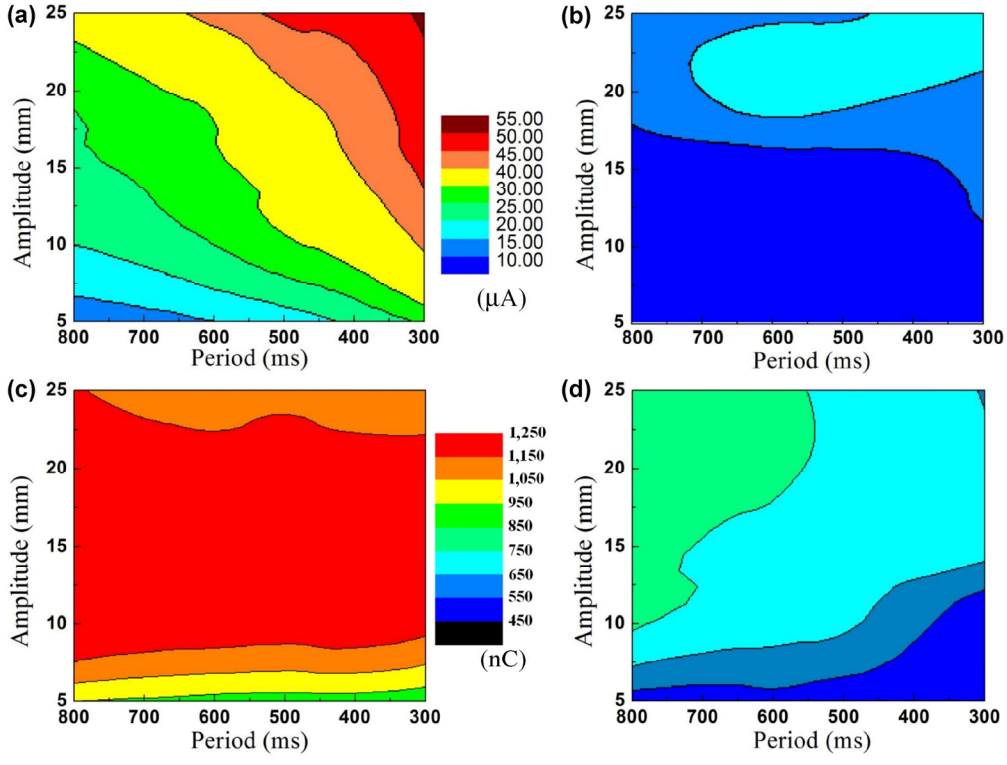

Figure 3 Color contour graphs about electrical measurement results of two TENGs under varied amplitude and motion period. The output current of (a) DI-TENG and (b) SI-TENG. Transferred charge quantity in a half cycle of (c) DI-TENG and (d) SI-TENG.

smaller velocity when more units of DI-TENG are integrated, since there is a positive correlation between the output current and the contact/separate velocity of its tribo-layers [23]. Therefore, the output current of DI-TENG seems to be smaller than other TENGs [18–23]. The total amount of transferred charges almost remains maximal between the amplitude of 7 and 22 mm in different periods for the DI-TENG, while it increases as the period and amplitude increases for the SI-TENG. Similarly, the maximum quantity of the transferred charges in a half period of the DI-TENG is 1.68 times as much as that of the SI-TENG. The quantity of transferred charges is small in low amplitude, which is attributed to less energy harvesting in low amplitude, and it reaches as high as 1.25 μC. Besides, the output voltage has been systematically investigated and the result is shown in Fig. S8 (in the ESM). The voltage–time waveform can also been found in Fig. S5(b) (in the ESM) and the maximum output voltage of DI-TENG is 418 V. On an average, the output voltage of the DI-TENG is 5.29 times as much as that of the SI-TENG.

The output current, voltage, and power under varied load resistance for the DI-TENG and SI-TENG driven by the linear motor in a motion period of 300 ms and amplitude of 25 mm are shown in Fig. 4(a) and 4(b). The current decreases and voltage increases with an increase in external load resistance. The output power of the DI-TENG reaches a maximum of 2.16 mW at a load of 2 MΩ, while that of the SI-TENG only reaches 0.24 mW. Figure 4(c) gives output voltage of DI/SI-TENG on changing amplitude and period in a 3D graph.

Benefiting from the spring steel based double-induction structure, DI-TENG has an advantage over SI-TENG. Particularly, the DI-TENG greatly improves output electricity without large displacement and big volume, which maximizes the space utilization under the contact/separation mode. With this great capacity, the TENG can sufficiently power a commercial calculator after the output current has been rectified by a bridge rectifier and can charge a 1 μF capacitor. As we can see from Fig. 4(d) and Video S1 (in the ESM), the calculator can be operated well with small

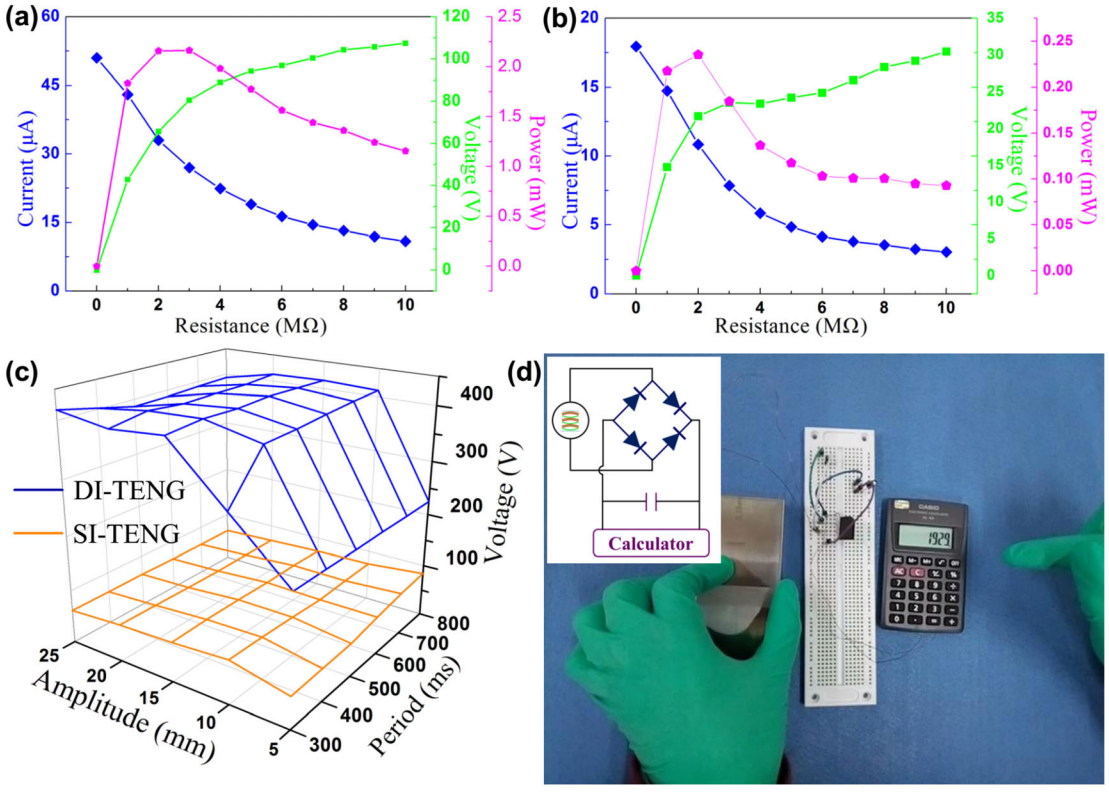

Figure 4 Output performance under different external loads of (a) DI-TENG and (b) SI-TENG. (c) 3D graph of varied output voltage on changing amplitude and period. (d) Digital photograph of a commercial calculator that is powered by the DI-TENG. Inset is the equivalent circuit for powering the calculator.

driving energy into the TENG. The inset is equivalent circuit of the whole working process. A door switch sensor based on the DI-TENG is further employed to demonstrate its great potential application. The sensor fabricated with 15 integrated units has higher output power and flexural property (Fig. S1 in the ESM). The operating circuit is elaborately designed in Fig. 5(a), while the sensor is fixed on the top of a door pivot, as shown in Fig. 5(b). When the door is being opened/closed, the sensor is driven to produce an output signal to the resistor (1 MΩ). The programmable microcontroller (STM32) detects the voltage on the resistor in real-time, and when it reaches a given value, the microcontroller sends out a signal to the composite transistor, which controls the pick-up of the relay to operate the on-off of an electric lamp. The insets in Fig. 5(b) are digital pictures of the complete circuit (left) and two working states (right), showing that the sensor can turn the mechanical signal into an electric signal, which might also be applied to other situations. By the above experiments, we can see that the DI-TENG has great output performance as well as potential application in smart home sensing, environmental monitoring, and electricity supply for personal electronic devices.

4 Conclusions

We have designed a double-induced-mode integrated triboelectric nanogenerator. By employing spring steel plates as skeleton and as electrodes, a small volume of DI-TENG could be achieved. The electrodes with two-side friction layers in the DI-TENG can greatly enhance the output performance, of which the output current, the transferred charges, and the output voltage is, respectively, 2.99 times, 1.68 times, and 5.29 times as much as that of the similar electrodes with single-side friction layer in the SI-TENG, which is commonly used in other integrated TENGs. The largest short-circuit current, open-circuit voltage, and transferred

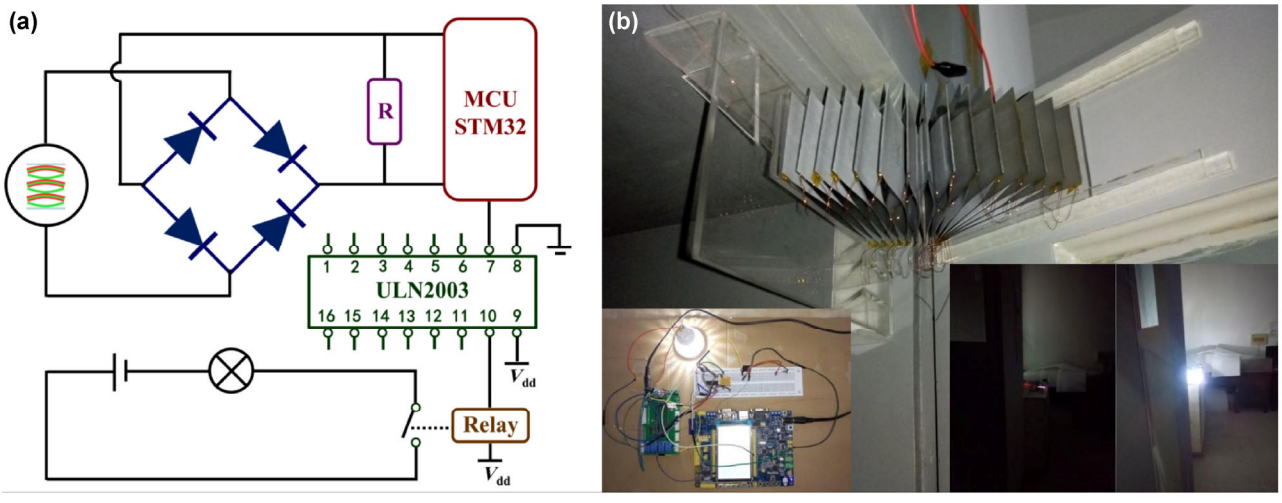

Figure 5 Demonstration of the DI-TENG as a door switch sensor. (a) The whole operating circuit. (b) Digital photograph of a DI-TENG based door switch sensor. The inset on the left is electrical network. The two insets on the right are two working states when the door is closed and open.

charges in a half period are 51 μA, 418 V, and 1.25 μC, respectively. With its unique structure and stretchable property, the fabricated DI-TENG can easily power a commercial calculator and can be applied to a door switch sensor. This study opens up the possibility of utilizing new materials into TENGs for extending its application scope.

Acknowledgements

This work is supported by National Natural Science Foundation of China (Nos. 51572040 and 51402112), Chongqing University Postgraduates' Innovation Project (No. CYS15016), the Fundamental Research Funds for the Central Universities (Nos. CQDXWL-2014-001 and CQDXWL-2013-012), and the National High-tech R&D Program of China (863 program) (No. 2015AA034801).

Electronic Supplementary Material: Supplementary material (Video S1 demonstrates a commercial calculator is driven by a DI-TENG with five units. Figure S1 demonstrates the digital photograph of DI-TENG with fifteen units under different conditions, Fig. S2 demonstrates the thickness exhibitions of the DI-TENG with different units, Fig. S3 demonstrates the complete schematic diagrams of charge distributions and current direction in separation and contact state, Fig. S4 demonstrates the charge generation procedure of DI-TENG, Fig. S5 demonstrates the current waveform and voltage waveform of the DI-TENG, Figs. S6 and S7 demonstrat the performance of the DI-TENG and SI-TENG, and Fig. S8. demonstrates the 2D graphs derived from the 3D surface graph in Fig. 4(c)) is available in the online version of this article at http://dx.doi.org/10.1007/s12274-016-1213-8.

References

[1] Evan, D. The internet of things: How the next evolution of the internet is changing everything. http://www.cisco.com/c/dam/en_us/about/ac79/docs/innov/IoT_IBSG_0411FINAL.pdf (accessed Jun 13, 2016).

[2] Wang, Z. L.; Song, J. H. Piezoelectric nanogenerators based on zinc oxide nanowire arrays. *Science* **2006**, *312*, 242–246.

[3] Qin, Y.; Wang, X. D.; Wang, Z. L. Microfibre-nanowire hybrid structure for energy scavenging. *Nature* **2008**, *451*, 809–813.

[4] Wu, N.; Cheng, X. F.; Zhong, Q. Z.; Zhong, J. W.; Li, W. B.; Wang, B.; Hu, B.; Zhou, J. Cellular polypropylene piezoelectret for human body energy harvesting and health monitoring. *Adv. Funct. Mater.* **2015**, *25*, 4788–4794.

[5] Beeby, S. P.; Tudor, M. J.; White, N. M. Energy harvesting vibration sources for microsystems applications. *Meas. Sci. Technol.* **2006**, *17*, R175–R195.

[6] Li, W. B.; Wu, N.; Zhong, J. W.; Zhong, Q. Z.; Zhao, S.; Wang, B.; Cheng, X. F.; Li, S. L.; Liu, K.; Hu, B. et al.

Theoretical study of cellular piezoelectret generators. *Adv. Funct. Mater.* **2016**, *26*, 1964–1974.

[7] Wang, L.; Yuan, F. G. Vibration energy harvesting by magnetostrictive material. *Smart Mater. Struct.* **2008**, *17*, 045009.

[8] Lu, S. N.; Liao, Q. L.; Qi, J. J.; Liu, S.; Liu, Y. C.; Liang, Q. J.; Zhang, G. J.; Zhang, Y. The enhanced performance of piezoelectric nanogenerator via suppressing screening effect with Au particles/ZnO nanoarrays Schottky junction. *Nano Res.* **2016**, *9*, 372–379.

[9] Fan, F. R.; Tian, Z. Q.; Wang, Z. L. Flexible triboelectric generator! *Nano Energy* **2012**, *1*, 328–334.

[10] Wang, Z. L.; Chen, J.; Lin, L. Progress in triboelectric nanogenerators as a new energy technology and self-powered sensors. *Energy Environ. Sci.* **2015**, *8*, 2250–2282.

[11] Liu, Y.; Niu, S. M.; Wang, Z. L. Theory of tribotronics. *Adv. Electron. Mater.* **2015**, *1*, 1500124.

[12] Cui, N. Y.; Liu, J. M.; Gu, L.; Bai, S.; Chen, X. B.; Qin, Y. Wearable triboelectric generator for powering the portable electronic devices. *ACS Appl. Mater. Interfaces* **2015**, *7*, 18225–18230.

[13] Guo, H. Y.; He, X. M.; Zhong, J. W.; Zhong, Q. Z.; Leng, Q.; Hu, C. G.; Chen, J.; Tian, L.; Xi, Y.; Zhou, J. A nanogenerator for harvesting airflow energy and light energy. *J. Mater. Chem. A* **2014**, *2*, 2079–2087.

[14] Xie, Y. N.; Wang, S. H.; Niu, S. M.; Lin, L.; Jing, Q. S.; Yang, J.; Wu, Z. Y.; Wang, Z. L. Grating-structured freestanding triboelectric-layer nanogenerator for harvesting mechanical energy at 85% total conversion efficiency. *Adv. Mater.* **2014**, *26*, 6599–6607.

[15] Tang, W.; Jiang, T.; Fan, F. R.; Yu, A. F.; Zhang, C.; Cao, X.; Wang, Z. L. Liquid-metal electrode for high-performance triboelectric nanogenerator at an instantaneous energy conversion efficiency of 70.6%. *Adv. Funct. Mater.* **2015**, *25*, 3718–3725.

[16] Zhu, G.; Zhou, Y. S.; Bai, P.; Meng, X. S.; Jing, Q. S.; Chen, J.; Wang, Z. L. A shape-adaptive thin-film-based approach for 50% high-efficiency energy generation through micro-grating sliding electrification. *Adv. Mater.* **2014**, *26*, 3788–3796.

[17] Weiss, P. S. A conversation with prof. Zhong Lin Wang, energy harvester. *ACS Nano* **2015**, *9*, 2221–2226.

[18] Zhu, G.; Pan, C. F.; Guo, W. X.; Chen, C.-Y.; Zhou, Y. S.; Yu, R. M.; Wang, Z. L. Triboelectric-generator-driven pulse electrodeposition for micropatterning. *Nano Lett.* **2012**, *12*, 4960–4965.

[19] Zhong, Q. Z.; Zhong, J. W.; Cheng, X. F.; Yao, X.; Wang, B.; Li, W. B.; Wu, N.; Liu, K.; Hu, B.; Zhou, J. Paper-based active tactile sensor array. *Adv. Mater.* **2015**, *27*, 7130–7136.

[20] Chen, J.; Guo, H. Y.; He, X. M.; Liu, G. L.; Xi, Y.; Shi, H. F.; Hu, C. G. Enhancing performance of triboelectric nanogenerator by filling high dielectric nanoparticles into sponge PDMS film. *ACS Appl. Mater. Interfaces* **2016**, *8*, 736–744.

[21] Zhong, J. W.; Zhu, H. L.; Zhong, Q. Z.; Dai, J. Q.; Li, W. B.; Jang, S.-H.; Yao, Y. G.; Henderson, D.; Hu, Q. Y.; Hu, L. B. et al. Self-powered Human-interactive transparent nanopaper systems. *ACS Nano* **2015**, *9*, 7399–7406.

[22] Zhong, J. W.; Zhong, Q. Z.; Hu, Q. Y.; Wu, N.; Li, W. B.; Wang, B.; Hu, B.; Zhou, J. Stretchable self-powered fiber-based strain sensor. *Adv. Funct. Mater.* **2015**, *25*, 1798–1803.

[23] Liu, G. L.; Xu, W. N.; Xia, X. N.; Shi, H. F.; Hu, C. G. Newton's cradle motion-like triboelectric nanogenerator to enhance energy recycle efficiency by utilizing elastic deformation. *J. Mater. Chem. A* **2015**, *3*, 21133–21139.

[24] Zhu, G.; Chen, J.; Liu, Y.; Bai, P.; Zhou, Y. S.; Jing, Q. S.; Pan, C. F.; Wang, Z. L. Linear-grating triboelectric generator based on sliding electrification. *Nano Lett.* **2013**, *13*, 2282–2289.

[25] Wang, S. H.; Lin, L.; Xie, Y. N.; Jing, Q. S.; Niu, S. M.; Wang, Z. L. Sliding-triboelectric nanogenerators based on in-plane charge-separation mechanism. *Nano Lett.* **2013**, *13*, 2226–2233.

[26] Zhang, C.; Zhou, T.; Tang, W.; Han, C. B.; Zhang, L. M.; Wang, Z. L. Rotating-disk-based direct-current triboelectric nanogenerator. *Adv. Energy Mater.* **2014**, *4*, 1301798.

[27] Yang, Y.; Zhang, H. L.; Chen, J.; Jing, Q. S.; Zhou, Y. S.; Wen, X. N.; Wang, Z. L. Single-electrode-based sliding triboelectric nanogenerator for self-powered displacement vector sensor system. *ACS Nano* **2013**, *7*, 7342–7351.

[28] Niu, S. M.; Liu, Y.; Wang, S. H.; Lin, L.; Zhou, Y. S.; Hu, Y. F.; Wang, Z. L. Theoretical investigation and structural optimization of single-electrode triboelectric nanogenerators. *Adv. Funct. Mater.* **2014**, *24*, 3332–3340.

[29] Meng, B.; Tang, W.; Zhang, X. S.; Han, M. D.; Liu, W.; Zhang, H. X. Self-powered flexible printed circuit board with integrated triboelectric generator. *Nano Energy* **2013**, *2*, 1101–1106.

[30] Wang, S. H.; Xie, Y. N.; Niu, S. M.; Lin, L.; Wang, Z. L. Freestanding triboelectric-layer-based nanogenerators for harvesting energy from a moving object or human motion in contact and non-contact modes. *Adv. Mater.* **2014**, *26*, 2818–2824.

[31] Guo, H. Y.; Leng, Q.; He, X. M.; Wang, M. J.; Chen, J.; Hu, C. G.; Xi, Y. A triboelectric generator based on checker-like interdigital electrodes with a sandwiched pet thin film for harvesting sliding energy in all directions. *Adv. Energy Mater.* **2015**, *5*, 1400790.

[32] Han, C. B.; Zhang, C.; Tang, W.; Li, X. H.; Wang, Z. L. High power triboelectric nanogenerator based on printed

circuit board (PCB) technology. *Nano Res.* **2015**, *8*, 722–730.

[33] Zhu, G.; Bai, P.; Chen, J.; Wang, Z. L. Power-generating shoe insole based on triboelectric nanogenerators for self-powered consumer electronics. *Nano Energy* **2013**, *2*, 688–692.

[34] Hou, T.-C.; Yang, Y.; Zhang, H. L.; Chen, J.; Chen, L.-J.; Wang, Z. L. Triboelectric nanogenerator built inside shoe insole for harvesting walking energy. *Nano Energy* **2013**, *2*, 856–862.

[35] Huang, T.; Wang, C.; Yu, H.; Wang, H. Z.; Zhang, Q. H.; Zhu, M. F. Human walking-driven wearable all-fiber triboelectric nanogenerator containing electrospun polyvinylidene fluoride piezoelectric nanofibers. *Nano Energy* **2015**, *14*, 226–235.

[36] Zheng, Q.; Shi, B. J.; Fan, F. R.; Wang, X. X.; Yan, L.; Yuan, W. W.; Wang, S. H.; Liu, H.; Li, Z.; Wang, Z. L. *In vivo* powering of pacemaker by breathing-driven implanted triboelectric nanogenerator. *Adv. Mater.* **2014**, *26*, 5851–5856.

[37] Lin, L.; Wang, S. H.; Xie, Y. N.; Jing, Q. S.; Niu, S. M.; Hu, Y. F.; Wang, Z. L. Segmentally structured disk triboelectric nanogenerator for harvesting rotational mechanical energy. *Nano Lett.* **2013**, *13*, 2916–2923.

[38] Zhu, G.; Chen, J.; Zhang, T. J.; Jing, Q. S.; Wang, Z. L. Radial-arrayed rotary electrification for high performance triboelectric generator. *Nat. Commun.* **2014**, *5*, 3426.

[39] Liu, G. L.; Liu, R. P.; Guo, H. Y.; Xi, Y.; Wei, D. P.; Hu, C. G. A novel triboelectric generator based on the combination of a waterwheel-like electrode with a spring steel plate for efficient harvesting of low-velocity rotational motion energy. *Adv. Electron. Mater.* **2016**, *2*, 1500448.

[40] Chen, J.; Yang, J.; Li, Z. L.; Fan, X.; Zi, Y. L.; Jing, Q. S.; Guo, H. Y.; Wen, Z.; Pradel, K. C.; Niu, S. M. et al. Networks of triboelectric nanogenerators for harvesting water wave energy: A potential approach toward blue energy. *ACS Nano* **2015**, *9*, 3324–3331.

[41] Choi, D.; Lee, S.; Park, S. M.; Cho, H.; Hwang, W.; Kim, D. S. Energy harvesting model of moving water inside a tubular system and its application of a stick-type compact triboelectric nanogenerator. *Nano Res.* **2015**, *8*, 2481–2491.

[42] Bai, P.; Zhu, G.; Lin, Z.-H.; Jing, Q. S.; Chen, J.; Zhang, G.; Ma, J. S.; Wang, Z. L. Integrated multilayered triboelectric nanogenerator for harvesting biomechanical energy from human motions. *ACS Nano* **2013**, *7*, 3713–3719.

[43] Yang, W. Q.; Chen, J.; Jing, Q. S.; Yang, J.; Wen, X. N.; Su, Y. J.; Zhu, G.; Bai, P.; Wang, Z. L. 3D stack integrated triboelectric nanogenerator for harvesting vibration energy. *Adv. Funct. Mater.* **2014**, *24*, 4090–4096.

[44] Li, X. H.; Han, C. B.; Zhang, L. M.; Wang, Z. L. Cylindrical spiral triboelectric nanogenerator. *Nano Res.* **2015**, *8*, 3197–3204.

[45] Yang, P.-K.; Lin, Z.-H.; Pradel, K. C.; Lin, L.; Li, X. H.; Wen, X. N.; He, J.-H.; Wang, Z. L. Paper-based origami triboelectric nanogenerators and self-powered pressure sensors. *ACS Nano* **2015**, *9*, 901–907.

[46] Wang, J.; Wen, Z.; Zi, Y. L.; Zhou, P. F.; Lin, J.; Guo, H. Y.; Xu, Y. L.; Wang, Z. L. All-plastic-materials based self-charging power system composed of triboelectric nanogenerators and supercapacitors. *Adv. Funct. Mater.* **2016**, *26*, 1070–1076.

[47] Zhang, L. M.; Xue, F.; Du, W. M.; Han, C. B.; Zhang, C.; Wang, Z. L. Transparent paper-based triboelectric nanogenerator as a page mark and anti-theft sensor. *Nano Res.* **2014**, *7*, 1215–1223.

[48] Xie, Y. N.; Wang, S. H.; Niu, S. M.; Lin, L.; Jing, Q. S.; Su, Y. J.; Wu, Z. Y.; Wang, Z. L. Multi-layered disk triboelectric nanogenerator for harvesting hydropower. *Nano Energy* **2014**, *6*, 129–136.